Tracking studies in the longitudinal phase space for the TESLA Damping Ring Design

Christopher Burnton
Deutsches Elektronen-Synchroton DESY, D-22603 Hamburg

02 July 1998

Abstract

The TESLA linear collider will require bunch lengths in the range of 0.3 to 0.7 mm at the interaction point (IP) for the different parameter sets presently under discussion.

In order to achieve this the bunches leaving the TESLA damping ring will pass a single stage bunch length compressor.

To keep the demands of the latter moderate, the TESLA damping ring needs to fulfil limitations in respect to the longitudinal phase space (in the range of 4 mm to a maximum of 1 cm for the bunch length and 0.1 percent for the energy spread).

The possibility of bunch lengthening effects and other instabilities due to wake fields need to be and have been studied.

The assumed wake fields of various components are presented and incorporated in a tracking method using a quasi-Green's function approach to simulate their effect on the longitudinal dynamics of the beam.

The results are compared to analytical estimations (ref. [1]).

1 Introduction

The TESLA linear collider design [2] foresees damping rings in order to reduce the beam phase space volumes down to the design emittance for collider operation. In case of the electron beam, using a laser rf-gun may pose an alternative.
The normalized emittance of the positron beam injected into the ring which is assumed to $\gamma\epsilon_i = 0.01\,\mathrm{m}$ leads to a necessary vertical emittance reduction factor of $2 \cdot 10^{-5}$. This in combination with a storage time equal to the cycle time T_c of 200 ms determines the vertical damping time and hereby the necessary energy loss per turn.

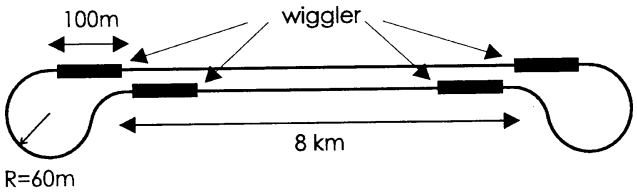

Figure 1: General layout of the "dog-bone"-shaped DR (ref. [2]).

In order to avoid the need for a costly additional ring tunnel, the TESLA damping ring is designed so that most of the lattice can be installed in the linac tunnel. Additional tunnels are only required for the two "loops" at the ends of the straight sections (see Figure 1).
The main complication which arises for the TESLA damping ring is due to the pulse structure of the linac. The train of the 1130 bunches per pulse has a length of 0.8 ms, or 240 km respectively. The bunch train will be therefore stored in a compressed mode, with a bunch spacing much smaller than in the linac.

1.1 Parameters

The parameters (for a one cm bunch) have been previously studied in detail in [1] and are to be found in Table 1. The ring and beam parameters are not in all cases exactly the same as those in the CDR report, i.e., the circumference is here 20 km compared to 17 km in the report (as it was taken from [1] and the studies began prior to the setting of design parameters).
The choice of the frequency, $f_{\rm rf} = 433\,\mathrm{MHz}$, is motivated by having an integer fraction of the main linac frequency and by the availability of high power klystrons ([2]).
The relative rms energy spread induced by synchrotron radiation is determined by the ring structure (see [3]):

$$\sigma_E^2 = \frac{<\Delta E^2>}{E^2} = \frac{C_q}{J_\epsilon}\gamma^2 \frac{\left\langle \frac{1}{\rho^3} \right\rangle}{\left\langle \frac{1}{\rho^2} \right\rangle}, \quad C_q \approx 3.84 \cdot 10^{-13}\mathrm{m} \tag{1}$$

where the damping partition number $J_\epsilon \approx 2$, ρ is the particle curvature radius in the magnetic field along the orbit.
As the radiation comes mainly from the wigglers with the piece-wise constant magnetic field $B_0 = 1.5\,\mathrm{T}$, the energy spread in the TESLA Damping Ring (DR) is circumference independent:

$$\sigma_E = \sqrt{\frac{C_q \gamma \mathrm{e} B_0}{J_\epsilon c m_0}} \approx 0.85 \cdot 10^{-3}\sqrt{B_0[T]} = 1.04 \cdot 10^{-3}. \tag{2}$$

Table 1: TESLA dog-bone damping ring parameters relevant for this study.

Parameter			units
Circumference	C	20	km
Rev. frequency	f_0	ca. 15	kHz
DC/bunch	I_b	0.09	mA
Energy	E	3.3	GeV
Loss per turn	U_0	12	MeV
Energy spread	σ_{E}	$1.04 \cdot 10^{-3}$	
RF-Voltage	$\widehat{V}$	24	MV
Overvoltage factor	q=e$\widehat{V}/U_0$	2.0	
for bunch rms length $\sigma_s = 1\,$cm:			
Synchr. tune	ν_s	0.087	
Mom. compaction	α	$2.7 \cdot 10^{-4}$	

In [1] it was assumed that the rms bunch length σ_s was fixed at approx. 1 cm. The choice of a certain overvoltage factor q, the ratio of the peak rf-voltage $\widehat{V}$ and the energy loss per revolution U_0:

$$q = \frac{1}{\sin\phi_s} = \frac{\mathrm{e}\widehat{V}}{U_0} \tag{3}$$

then determines the necessary values of the momentum compaction factor α and the synchrotron tune ν_s to obtain the wished bunch length. This can be easily seen by studying the relationships

$$\sigma_s = \sigma_E \frac{\alpha C}{2\pi\nu_s} \tag{4}$$

and

$$\nu_s^2 = \frac{\alpha h \mathrm{e}\widehat{V}\cos\phi_s}{2\pi E}. \tag{5}$$

The above h is the harmonic number, relating the revolution frequency to the rf-frequency, $f_{\mathrm{rf}} = h \cdot f_0$.
The advantages and disadvantages of smaller and larger overvoltage factors q are discussed in [1]. For sake of definiteness q was chosen to be two whereby α and ν were determined.
Here q has been left at two, but the momentum compaction has been looked upon as variable to obtain different rms bunch lengths σ_s and to study the wake field effects.

The above relationships (4) and (5) correspond to the following two:

$$\sigma_s^2 = \frac{\sigma_E^2 \alpha C^2 E}{2\pi h U_0 \sqrt{q^2-1}}, \tag{6}$$

$$\nu_s^2 = \frac{\alpha h U_0 \sqrt{q^2-1}}{2\pi E}. \tag{7}$$

2 Simulation Technique

The simulation is based upon the usage of macroparticles and the incorporation of wake field effects into the equations of motion with the help of quasi-Green's functions (see [4]).

A bunch is represented by a variable number N_{par} of macroparticles (τ_k, ε_k) where

τ_k particle position in time with origin at zero of the main RF,
ε_k particle energy deviation from nominal energy E.

The tracking equations in the program are such that it is possible to define different sections within the machine and track during one turn from one sector to another. The equations of motion are described by practically the same equations as given here for a full revolution for simplicity where the phase space coordinates on turn $n+1$ are related to those on turn n by

$$\tau_k^{n+1} = \tau_k^n + \frac{\alpha \mathrm{T}_0}{\mathrm{E}} \varepsilon_k^n - \frac{\alpha \mathrm{T}_0 \mathrm{U}_0}{2\mathrm{E}} \tag{8}$$

$$\varepsilon_k^{n+1} = \varepsilon_k^n + \mathrm{e} \sum_{i=1}^{m} \widehat{\mathrm{V}}_i \sin(\omega_{\mathrm{rf,i}} \tau_k^{n+1} + \phi_i) - \mathrm{U}_0 - \frac{2\mathrm{T}_0}{\mathrm{T}_\varepsilon} \varepsilon_k^n + 2\sqrt{\frac{\mathrm{T}_0}{\mathrm{T}_\varepsilon}} \sigma_{0\varepsilon} R + \mathrm{e} W(\tau_k^{n+1}) \tag{9}$$

with

α	momentum compaction
T_0	beam revolution period
E	nominal energy
U_0	average synchrotron radiation loss per turn
$\mathrm{e}\widehat{\mathrm{V}}_i$	peak energy gain from the RF i
$\omega_{\mathrm{rf,i}}$	angular frequency of the RF i
ϕ_i	phase off-set from main RF (with index $i = 1$, $\phi_1 = 0$)
T_ε	radiation damping time for energy oscillations
$\sigma_{0\varepsilon}$	natural energy spread of the beam
R	Gaussian distributed random number with mean = 0 and rms = 1
W	wake field

Memory effects due to resonant modes in cavities are not included. The second to last term on the right hand side of the second equation describes the energy variation due to quantum excitation by photon emission.
The third term on the right hand side of the first equation reflects the continuous radiation loss, here between two successive turns. Due to this term a synchronous particle has a non-zero amplitude.
It is interesting to note that linearization of the rf-potential and neglection of the damping and quantum excitation terms lead however then to a symplectic mapping, in this special case via the leap-frog integration method.
When tracking with e.g. p identical sections T_0 is replaced for example by $\mathrm{T}_0^j = \mathrm{T}_0/p$.
Note, that in the TESLA DR there is only one rf-frequency although the above equations show the possibility of having different frequencies.

Instead of using Green's functions (delta-wakes) to calculate the wake fields quasi-Green's functions are used, the wakes of Gaussian bunches with a smaller rms value than the bunch studied.
The basic idea behind this technique is the following relationship between the wakes of two Gaussian bunches due to the one and same delta wake.

$$\begin{aligned} \mathrm{W}_{\sigma_i}(s) &= \int_{-\infty}^{\infty} dz\, \lambda_{\sigma_i}(s-z)\, \mathrm{W}_{\delta}(z), \quad i = 1,2 \\ \Rightarrow \mathrm{W}_{\sigma_2}(s) &= \int_{-\infty}^{\infty} dz\, \lambda_{\sqrt{\sigma_2^2-\sigma_1^2}}(s-z)\, \mathrm{W}_{\sigma_1}(z). \end{aligned}$$

Note

$$\sqrt{\sigma_2^2 - \sigma_1^2} = \sigma_2 \sqrt{1 - \left(\frac{\sigma_1}{\sigma_2}\right)^2} \approx \sigma_2, \quad \sigma_1 \ll \sigma_2,$$

so that

$$\mathrm{W}_{\sigma_2}(s) \approx \int_{-\infty}^{\infty} dz\, \lambda_{\sigma_2}(s-z)\, \mathrm{W}_{\sigma_1}(z). \tag{10}$$

Figure 2: Macroparticle binning.

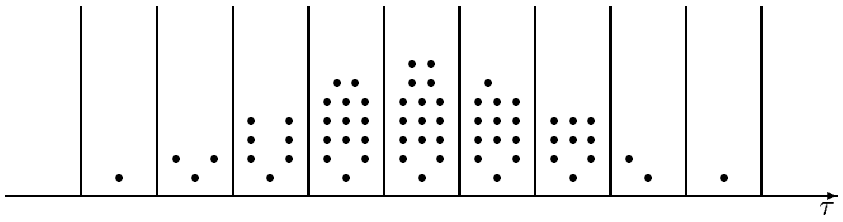

The numerical approximation has an acasual part to it as $\mathrm{W}_{\sigma_1}(z) \not\equiv 0$ for $z < 0$. In the following the abbreviation QGF will stand for quasi-Green's function and mean any wake which is being used instead of the Green's function, as in the above case $\mathrm{W}_{\sigma_1}(z)$.

To determine the wake field seen by a macroparticle a binning technique is used. The bunch represented by the N_{par} macroparticles is divided into bins with a pre-defined constant width.
Then $\tau_{\mathrm{c}}(i)$, the centre of mass for every bin i, and $n_{\mathrm{b}}(i)$, the number of particles in bin i, are determined.
The wake field effect on each bin is calculated as:

$$W_{\mathrm{b}}(i) = \frac{Q}{N_{\mathrm{par}}} \sum_{j=1}^{N_{\mathrm{bin}}} n_{\mathrm{b}}(j) \cdot \mathrm{QGF}(\tau_{\mathrm{c}}(i) - \tau_{\mathrm{c}}(j)) \tag{11}$$

which corresponds to

$$W_{\lambda}(s) = \int_{-\infty}^{s} dz\, \lambda(z)\, W_{\delta}(s-z)$$

with λ a normalized line charge density, i.e. $\int_{-\infty}^{\infty} dz\, \lambda(z) = 1$ and with the delta-wake or Green's function $W_{\delta}(z)$.
The wake field seen by a macroparticle (τ_k, ε_k) is then calculated by linear interpolation

$$W(\tau_k) = W_{\mathrm{b}}(i) \cdot (1 - \Delta\tau) + W_{\mathrm{b}}(i+1) \cdot \Delta\tau, \tag{12}$$

where

$$\Delta\tau = \frac{\tau_k - \tau_{\mathrm{c}}(i)}{\tau_{\mathrm{c}}(i+1) - \tau_{\mathrm{c}}(i)} \quad \text{and} \quad \tau_{\mathrm{c}}(i) \le \tau_k < \tau_{\mathrm{c}}(i+1).$$

Therefore there is no artificial jump of the wake fields seen by the macroparticles due to the binning, i.e. the transition between two bins is continuous.
In a few cases the wake calculation has been changed by doing the following: the number of particles per bin $n_{\mathrm{b}}(i)$ is replaced by the average over the bins $i-m$ to $i+m$, i.e. $\tilde{n}_{\mathrm{b}}(i) = (n_{\mathrm{b}}(i-m)+\ldots+n_{\mathrm{b}}(i)+\ldots n_{\mathrm{b}}(i+m))/(2m+1)$, the centre of the mass is replaced by the middle of the bin. This was done to test the influence of statistical fluctuations concerning the number of particles per bin. The above will be referred to as a "smoothed" calculation using $2m+1$ bins.
Figure 3 compares the inductive wake, $Z(w) = i\omega L$, of a 1 cm Gaussian bunch in the dog-bone with that obtainable by convolution using the wake of a 3 mm Gaussian bunch as a QGF. The convolution has been calculated by numerical approximation of

$$\mathrm{W}_{\sigma_2}^{\sigma_1}(s) = \int_{-\infty}^{\infty} dz\, \lambda_{\sigma_2}(s-z)\, \mathrm{W}_{\sigma_1}(z) \tag{13}$$

which corresponds to letting $N_{\mathrm{bin}} \to \infty$ and $N_{\mathrm{par}} \to \infty$ when using the binning technique.

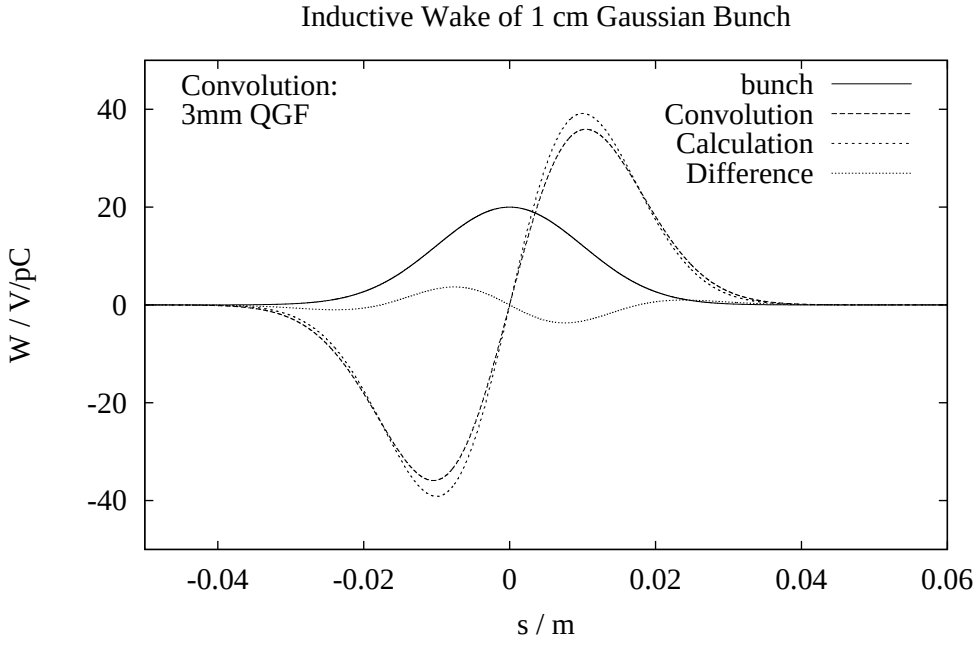

Figure 3: The assumed inductive wake of a 1 cm Gaussian bunch in the damping ring (L = 0.18 μH). The term "calculation" refers here to the true inductive wake and the term "convolution" to the wake obtained by using Eq. (13). "Difference" is just the difference between the two wakes.

In the case of an inductive wake, $W_\delta(s) = \hat{G}_0 \cdot \delta'(s)$ where $\hat{G}_0 = -c^2 L$, Eq. (13) can be solved analytically:

$$W_\sigma^{\sigma_{\rm QGF}}(s) = -\frac{\hat{G}_0}{\sigma_1^2}\kappa\frac{1}{\sqrt{2\pi}}\exp(-\frac{s^2}{2\sigma^2})\frac{s}{\sigma}(1+\kappa^2)^{-3/2}\exp\left(\frac{\frac{s^2}{2\sigma^2}}{1+\kappa^2}\right) \qquad (14)$$

with $\kappa = \sigma/\sigma_{\rm QGF}$.
The relative error of the maximum absolute wake ($s = \pm\sigma$) is

$$e(\kappa) = 1 - \kappa^3(1+\kappa^2)^{-3/2}\exp\left(\frac{1}{2(1+\kappa^2)}\right). \qquad (15)$$

A number of examples are given in Table 2.

κ	1	2	5/3	2.5	3.3	5	10
$e(\kappa)$ [%]	54.6	20.9	28.0	14.2	8.4	3.9	1.0

Table 2: The relative error of the maximum absolute wake for an inductive wake as a function of the relative width κ of the studied bunch and the QGF.

The following will apply in future to all figures similar to Figure 3 in the paper unless otherwise stated. The abbreviations "Conv" and "Calc" will stand for convolution, respectively calculation (in this case it was the real value as the inductive wake can be calculated analytically). "Diff" will abbreviate difference and be simply the difference between the convolution and the calculation.

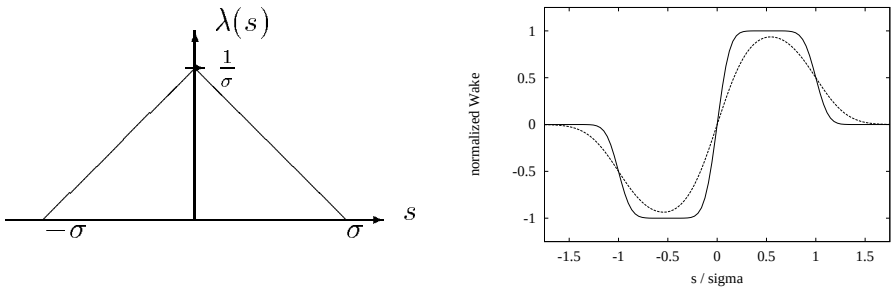

Figure 4: A bunch with the form of an isosceles triangle with the base 2σ and its wake as calculated using a Gaussian QGF, $\kappa = 10$ solid line, $\kappa = 4$ dashed line ($\kappa = \sigma/\sigma_{\mathrm{QGF}}$).

A further purely theoretical example is that of an inductive wake of a bunch with the form of an isosceles triangle with the base 2σ and

$$W_{\triangle,\sigma}(s) = \mathrm{sign}(s)\frac{1}{\sigma^2} \cdot \widehat{\mathrm{G}}_0.$$

Equation (10) leads to

$$W_{\triangle,\sigma}^{\sigma_{\mathrm{QGF}}}(s) = \frac{-\widehat{\mathrm{G}}_0}{\sigma^2}\left(\mathrm{erf}\left(\frac{s}{\sqrt{2}\sigma_{\mathrm{QGF}}}\right) - \frac{1}{2}\mathrm{erf}\left(\frac{s-\sigma}{\sqrt{2}\sigma_{\mathrm{QGF}}}\right) - \frac{1}{2}\mathrm{erf}\left(\frac{s+\sigma}{\sqrt{2}\sigma_{\mathrm{QGF}}}\right)\right).$$

Due to the discontinuity of the step function the particles in the middle of the bunch see naturally a large mistake, nevertheless that total error in respect to the whole bunch drops drastically with increasing κ (see Figure 4).
One advantage of the binning is that the evaluation of Eq. (11) is $\sim N_{\mathrm{bin}}^2$ operations where as the corresponding equation to Eq. (11) would otherwise lead to a term $\sim N_{\mathrm{par}}^2$. Naturally one must still take into account the filling of the bins (the particles are pre-sorted which is $\sim N_{\mathrm{par}} \log N_{\mathrm{par}}$) and the later interpolation (Eq. (12)) but this amounts to obviously less for larger particle numbers.

3 Analytical estimation of collective effects

3.1 The Haissinski Equation

The Haissinski equation (see [5]) is a non-linear integral equation describing, in a suitable phase space, the evolution of the longitudinal particle density distribution of a bunch. The parabolic potential-well formed by the accelerating rf-voltage is distorted by the longitudinal wake field, and as a result the longitudinal beam distribution is deformed.
The beam current distribution below the turbulent threshold, calculated with the Haissinski equation, is given by (see [6])

$$I(t) = K \exp\left(\frac{1}{\sigma_{t0}^2 \mathrm{e}|\dot{V}_{RF}|}\int_0^t dt' \ [\mathrm{e}V_{RF}(t') - U_0 + \mathrm{e}V_{ind}(t')]\right), \qquad (16)$$

where σ_{t0} and $\dot{V}_{RF}$ are the natural bunch length and the slope of the rf-voltage at the position of the bunch. Furthermore, V_{ind}, the transient induced voltage with $t = 0$ the synchronous position for the low current beam, is given by

$$V_{ind}(t) = -\int_0^\infty dt' W_\delta(t') I(t - t') \qquad (17)$$

with $W_\delta(t)$ a Green's function of the longitudinal wake field. The value of the normalized constant K in Eq. (16) is defined as the complete integral of $I(t)$ is equal to Q, the total charge of the bunch.
When the rf-potential is linearized Eq. (16) takes the form

$$I(t) = K \exp\left(-\frac{t^2}{2\sigma_{t0}^2} + \frac{1}{\dot{V}_{RF}\sigma_{t0}^2}\int_0^t dt' V_{ind}(t')\right). \qquad (18)$$

By taking the derivative of both sides of Eq. (18) one obtains

$$\frac{\dot{I}}{I} = -\frac{t}{\sigma_{t0}^2} + \frac{V_{ind}}{\dot{V}_{RF}\sigma_{t0}^2}. \qquad (19)$$

Either Eq. (18) or (19) can be used to estimate the bunch distribution and length due to the distortion of the rf-potential by the wake fields.
When the impedance of the ring is assumed to be purely inductive, i.e. when the induced voltage is given by

$$V_{\mathrm{ind}} = -L\frac{dI}{dt} \qquad (20)$$

with a constant inductance L, Eq. (19) can be written as

$$\frac{dy}{dx} = -\frac{xy}{1+y} \qquad (21)$$

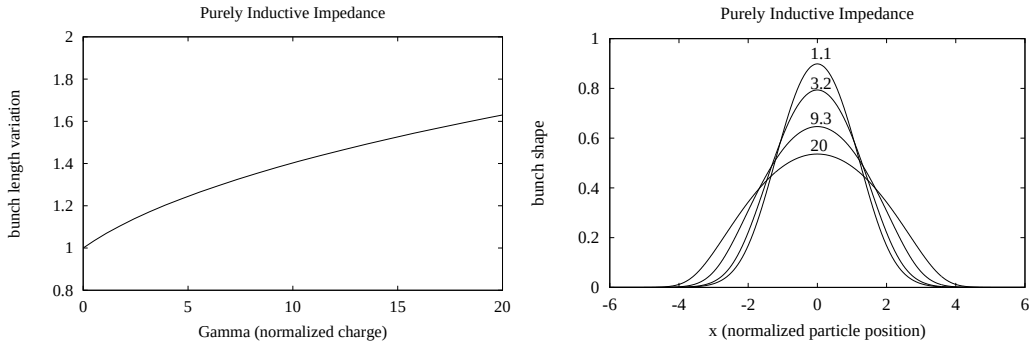

Figure 5: (a) The bunch length variation as a function of normalized bunch charge Γ and (b) the bunch shape for several values of Γ.

with the variables of $x = t/\sigma_{t0}$, $y = LI/\dot{V}_{RF}\sigma_{t0}^2$ (see [6] or also [7]). Here, it is possible to define the normalized charge Γ, the integral of y, as follows

$$\Gamma = \int_{-\infty}^{\infty} dx\, y = \frac{LQ}{\dot{V}_{RF}\sigma_{t0}^3}. \tag{22}$$

Γ is therefore inverse proportional to $\alpha^{3/2}$ (see Eq. (6)).
The numerical solution of Eq. (21) is shown in Figure 5 for several values of Γ. The charge distribution for a perfect inductor is symmetric about $x = 0$ and it is almost the same as the Gaussian distribution at low intensity regions. On the other hand, it is apparent that the solution of Eq. (21) is rather a parabolic than Gaussian distribution whenever $y \gg 1$. The σ_x values of Gaussian function for various Γ are shown in Figure 5. Figure 5 shows that σ_x varies like as linear for small current regions.
One should note that the approximation formula used in [1]

$$\frac{\Delta\sigma_s}{\sigma_s} \approx \frac{LQ}{2\sqrt{2\pi}\dot{V}_{RF}\sigma_{t0}^3} = \frac{\Gamma}{2\sqrt{2\pi}} \tag{23}$$

does not confer to the above results. Although Eq. (23) is also based on the Haissinski equation (18) the approximations made in the derivation of the formula (see [8]) lead to an over-estimation of the bunch lengthening effect (for small Γ by approximately a factor two).

The case of a purely capacitive impedance leads to an integro-differential equation. Its numerical solution shows that the bunches remain essentially Gaussian, but with a reduced length (see [9]).

The Haissinski equation for a purely resistive impedance $Z(w) = R$ can be solved analytically (see [9], [10]), the solution looks like a Gaussian with a widened centre part.

3.2 Microwave instability threshold

A further cause for bunch lengthening can be mode coupling (see [10]).
At higher bunch currents the bunch lengthening deviates significantly from the scaling of potential-well distortion. Associated with this lengthening is also an increase in the energy spread.
The Boussard criterion ([11]) is generally used as an analytical estimation of the threshold of the microwave longitudinal instability (as was done in [1]). It relates the effective broadband impedance and the beam and ring parameters:

$$\left(\frac{Z}{n}\right)_{\text{eff}}^{\text{thr}} = \frac{\sqrt{2\pi}\alpha(E/e)\sigma_E^2\sigma_s}{I_b R}, \tag{24}$$

where $n = (\omega/\omega_0) = \omega R/c = wC/(2\pi c)$ is the mode number.
Using Eq. (6):

$$\left(\frac{Z}{n}\right)_{\text{eff}}^{\text{thr}} = \frac{2\pi\alpha^{3/2}(E/e)^{3/2}\sigma_E^3}{I_b\sqrt{h(U_0/\text{e})}(q^2-1)^{1/4}}. \tag{25}$$

For the parameters of the TESLA DR one obtains

$$\left(\frac{Z}{n}\right)_{\text{eff}}^{\text{thr}} = 1.94\cdot 10^4\cdot\alpha^{3/2}\,[\Omega], \tag{26}$$

i. e. 86 $m\Omega$ for the dog-bone (as in Table 1: $\alpha = 2.7\cdot 10^{-4}$).
One should note however that the above formula only holds for long bunches (see [12]) and therefore is not necessarily correct in the studied cases.

4 Impedance Model

4.1 Sources of Inductive Impedance

The impedance of a ring may be estimated as the sum of the impedances of its components, such as bellows, BPMs, kickers, vacuum ports, tapers, etc. Most of these elements present discontinuities having an impedance covering frequencies much higher than the frequencies within the bunch spectrum, and, therefore, they give rise to a mostly inductive impedance (see [1], [10, p. 72-5]).
The total inductive impedance Z/n of the dog-bone DR was estimated by Shiltsev to be 17 mΩ, corresponding to an inductance L of $1.8\cdot 10^{-7}$ H, where the major contribution came from the bellows with 7.5 mΩ. This was based on the assumption that the bellows would be spaced on average every eight metres and where the inductance of the shielded bellows at the B-Factory (see [13]) was taken and scaled to the radius 5 cm.

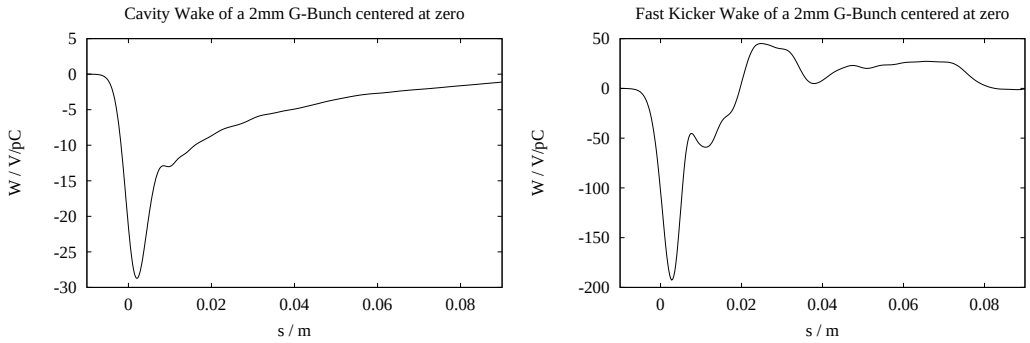

Figure 6: (a) Cavity and (b) Fast Kicker Wake of a 2 mm Gaussian Bunch.

One should note that whether an object is inductive or capacitive depends critically on the length of the driving charge. Vacuum chamber objects appear more inductive to longer bunches, more capacitive to shorter bunches ([14]). Therefore the above estimation might be not quite correct anymore for the two smaller bunch lengths studied.
For the simulation advantage is taken of the fact that an inductive impedance $Z = -i\omega L$ corresponds to a wake field which is inversely proportional to the derivative of the charge distribution:

$$W(s) = -L \cdot c^2 \lambda'(s) \tag{27}$$

In case of a Gaussian bunch (centred at zero) this leads to

$$W(s) = \frac{Lc^2 s}{\sqrt{2\pi}\sigma_s^3} \exp\left(-\frac{s^2}{2\sigma_s^2}\right) \tag{28}$$

which can be easily computed and used as a quasi-Green's function. The absolute wake maximum is reached at $s = \pm\sigma_s$ and is inverse proportional to σ_s^2.
In the presented simulation studies the wakes of bunches with σ_s equal to 0.5 mm, 1 mm, and 2 mm were used.

4.2 Resistive Wall

An aluminium vacuum chamber with a conductivity $\sigma_0 = 3.5 \cdot 10^7 \Omega^{-1} m^{-1}$, as proposed in the CDR, is assumed.
In the straight sections the pipe will have a radius of $b = 5$ cm, in the wiggler section (2 % of the circumference) a radius of $b = 1$ cm, and in the arcs ($\sim$ 6 % of circumference) $b = 3$ cm.
The longitudinal monopol resistive wall impedance of a round pipe in the long-range approximation reads (see [15]):

$$\bar{Z}_{0,\parallel}(k) = \frac{Z_0 \zeta_0^{3/2}}{4\pi b^2} \sqrt{|k|}(1 - i\,\mathrm{sign}(k)) \tag{29}$$

with the characteristic length

$$\zeta_0 = \left(\frac{2b^2}{Z_0\sigma_0}\right)^{1/3} \tag{30}$$

and $k = \omega/c$.
The corresponding wake field for a Gaussian charge distribution ($\hat{\lambda}(k)$ denotes the Fourier transform) is

$$W_{\|}(s) = -\frac{c}{2\pi}\int_{-\infty}^{\infty} dk\, \bar{Z}_{0,\|}(k)\hat{\lambda}(k)e^{-iks} \tag{31}$$

$$= -\frac{Z_0 c\zeta_0^{3/2}}{8\pi^2 b^2}\int_{-\infty}^{\infty} dk\,(1-\mathrm{sign}(k))\sqrt{|k|}e^{-k^2\sigma_s^2/2}e^{-iks} \tag{32}$$

$$= \frac{c}{4\pi b}\sqrt{\frac{Z_0}{\sigma_0}}\frac{1}{\sigma_s^{3/2}}\left|\frac{u}{2}\right|^{3/2}\{I_{1/4} - I_{3/4} + \mathrm{sign}(u)(I_{-1/4} - I_{3/4})\}e^{-u^2/4} \tag{33}$$

where u is a normalized distance between the bunch centre and the position of the test charge

$$u = \frac{s}{\sigma_s} \tag{34}$$

and the arguments of the Bessel functions I_ν are $u^2/4$.
The amplitude of the wake field relates to the radius b, the bunch length σ_s, and the conductivity σ_0 as

$$W_{\|} \propto b^{-1}\sigma_0^{-1/2}\sigma_s^{-3/2}. \tag{35}$$

For the simulation formula (33) has been used to calculate the quasi-Green's function up to the distance $u = 50$; beyond that a numerical calculation of the integral (32) in the form

$$W_{\|}(s) = \frac{-c\sqrt{Z_0/\sigma_0}}{2^{3/2}\pi^2 b\sigma^{3/2}}\int_0^{\infty} d\tilde{k}\sqrt{\tilde{k}}e^{-\tilde{k}^2/2}(\cos(\tilde{k}u) - \sin(\tilde{k}u)) \tag{36}$$

has been used.
To estimate the broad band impedance (see [1, 13]) note that (29) is equivalent to

$$\bar{Z}_{0,\|}(\omega) = \frac{1}{2\pi b}\sqrt{\frac{\mu_0|\omega|}{2\sigma_0}}(1 - i\mathrm{sign}(\omega)). \tag{37}$$

whereby one obtains

$$\left(\frac{\bar{Z}_{0,\|}}{n}\right) = \frac{Z_0\delta(\omega)}{2bC}(1 - i\mathrm{sign}(\omega)) \tag{38}$$

$$= \frac{\sqrt{Z_0}}{2b\sqrt{\pi C\sigma_0 n}}(1 - i\mathrm{sign}(\omega)) \tag{39}$$

where the skin depth $\delta(\omega) = \sqrt{2/(\mu_0 \sigma_0 \omega)}$.
At bunch frequencies $k\sigma_s = \omega\sigma_s/c \simeq 1$, i.e. $n_{\text{eff}} \sim R/\sigma_s$, the effective broad-band contribution can be estimated to be

$$\left(\frac{\bar{Z}_{0,\|}}{n}\right)_{\text{eff}} = \frac{\sqrt{Z_0 \sigma_s}}{\sqrt{2\sigma_0} bC}(1-i). \tag{40}$$

The broad band impedance for the dog-bone can therefore be estimated to be about $(Z/n)^W_{\text{eff}} \approx (1-i) \cdot 5.2\, m\Omega$ ($\alpha = 2.7 \cdot 10^{-4}$, $\sigma_s = 1\,\text{cm}$).

4.3 Cavities

The exact geometry of the RF cavities for the TESLA DR is not known yet. For this study eight 4-cell superconducting cavities, such as installed at HERA but scaled in frequency from 500 MHz to 433 MHz have been assumed (see Figure 7). The longitudinal wake fields of Gaussian bunches with σ_s equal to 2 and 3 mm have been calculated with the MAFIA T2 program (using the indirect integration method, therefore the addition of the junction and the beam pipe on both ends of the 4-cell cavity) and have been used as QGFs (see Figure 6). The wake of the 1 mm Gaussian bunch has been smoothed; for the calculation wake of the 0.5 mm Gaussian bunch only one cell has been used.
In [16, p. 127] it is stated that they expect the microwave instability threshold to be higher than that given by the Boussard criterion when the major contribution to an impedance is capacitive.

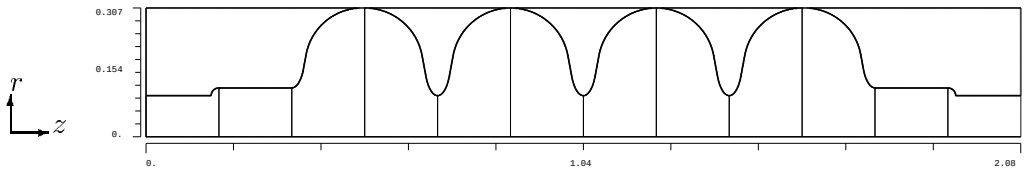

Figure 7: Schematic view of a 4-cell cavity.

In [1] the cavity broad band impedance was estimated by using the diffraction model for one-cell cavities.

$$\left(\frac{Z}{n}\right)_{\text{cav}} \approx (1+i) \cdot \frac{1.6\,[\text{m}\Omega]}{C\,[\text{km}]} \tag{41}$$

for $\sigma_s = 1\,\text{cm}$ and with the factor 1.45 for $\sigma_s = 5\,\text{mm}$.
This leads to a total effective cavity impedance (assumption 38 cavities) of $(Z/n)_{\text{cav}} \approx (1+i) \cdot 3\,\text{m}\Omega$, respectively 2.75 m$\Omega$.

4.4 Fast Kicker

For the impedance model the installation of 40 very fast kickers has been assumed. A description of the very fast counter travelling wave kickers which are intended to be used for the extraction of the bunches can be found in [17].
The wakes seen by a 1 cm and a 5 mm Gaussian bunch passing a fast kicker (multiplied by the factor 40) can be seen in Figure 12. They were calculated using the MAFIA T3 module [18].

$\lvert W_{\max}\rvert$ / 10^{12}V/C	4.81	3.55	2.85	2.45	1.43
σ_s / mm	2	3	4	5	10

Table 3: Maximum absolute wake of various Gaussian bunches.

According to the data in Table 3 the maximum absolute wake created by a Gaussian bunch passing a fast kicker varies approximately as

$$|W_{\max}^{\mathrm{FK}}| \sim \frac{1}{\sigma_s^{3/4}}. \tag{42}$$

The fast kickers were not accounted for in [1].

5 Simulation Results

For the simulation different numbers of macroparticles, number of sections (1 and 2), and different quasi-Green's functions for the various wakes (the rms bunch lengths varied between $\sigma_s = 0.5\,\mathrm{mm}$, 1 mm, 2 mm, and 3 mm) were used. The rms values for the bunch length and the energy spread per run were calculated as the average values over the last 500 of the 3000 turns for which the simulation was run (this being approximately equivalent to eleven damping times and the cycle time). When using two sections ($N_{\mathrm{sec}} = 2$) the dog-bone has been divided into two practically identical parts with the difference being that the rf-power is submitted only in the first section. The impact on the wake field calculation is explained in the appropriate places.
The four wake components have in part also been studied individually.
Table 4 shows the maximum relative weighted error (relative to the maximum wake) when comparing the results of Eq. (13) for a number of QGFs with the true or calculated wakes of a 5 mm and 1 cm Gaussian bunch.
In case of the actual simulation one must not forget that one has a limited number of particles and bins. Nevertheless for example a random Gaussian distribution of a 100 000 particles and a bin width of 0.2 mm delivers for the cavity and fast kicker results which are principally identical with the above

QGF	IN			RW			CV		FK	$\sum$
σ_s / mm	0.5	1	2	0.5	1	2	1	2	2	
5 mm bunch	1.1			0.8			1.7		4.9	1.7
		4.2			3.0		1.7		4.9	3.4
			15.0			10.9		4.0	4.9	11.1
1 cm bunch		1.1			0.8		0.8		1.3	1.1
			4.2			3.0		1.3	1.3	2.7

Table 4: Maximum relative weighted error in [%] (relative to the maximum wake) using the numerical calculaton of Eq. (13) for the inductive (IN), resistive wall (RW), cavity (CV), fast kicker (FK), and the combined (total) wake ($\sum$).

when studying the 5 mm bunch. In case of the resistive wall and inductive wake the results deteriorate noticeably. The convolution of the 0.5 mm resistive wall wake with a 5 mm Gaussian bunch can lead to a maximum relative weighted error of ca. 3–4 %, that of the inductive wake for the 0.5 mm and 1 mm QGF to an error of 9–15 %, respectively 8 %.
Note that the values of the resistive wall and the inductive wake vary far more strongly than those of the fast kicker and cavity wakes.

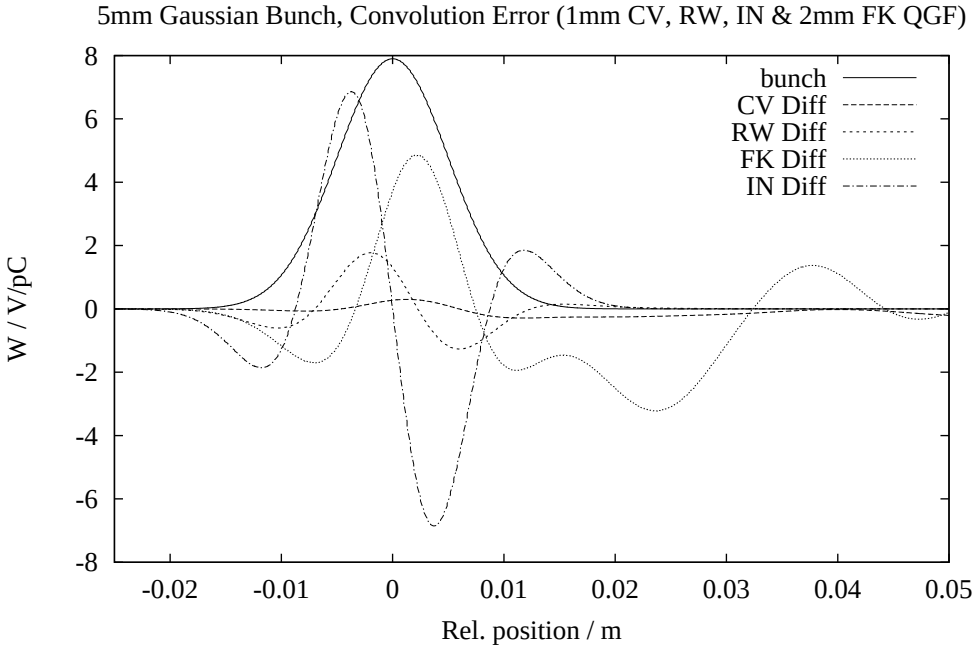

Figure 8: Convolution error using the 1 mm cavity (CV), resistive wall (RW), and inductive (IN) wake, and the 2 mm fast kicker (FK) wake to calculate the wake of a 5 mm Gaussian bunch.

The zero current rms bunch lengths for three studied momentum compaction factors are to be found in Table 5.

α	σ_s / cm	σ_ϵ / MeV
$5 \cdot 10^{-5}$	0.44	3.44
$7 \cdot 10^{-5}$	0.52	3.44
$27 \cdot 10^{-5}$	1.01	3.44

Table 5: Zero current rms bunch length and energy spread for the studied cases.

5.1 Inductive Wake

At the design current the inductive wake leads for the momentum compaction factor $\alpha = 5 \cdot 10^{-4}$ to a bunch lengthening of ca. 30 %. It can be fully understood by the Haissinski equation.
The rise in the rms energy spread at higher currents when using one section ($N_{\text{sec}} = 1$) seems to be due to a numerical instability as can be seen from the results when using two sections, i.e. an intermediate calculation step. As the inductive impedance is spread more or less evenly over the ring the macroparticles are appointed in both sections half of the total inductance value. This seems to be a more realistic approach than when using one section and interestingly the energy rise vanishes.

	$N_{\text{sec}} = 1$		$N_{\text{sec}} = 1$ smooth: 7		$N_{\text{sec}} = 2$		Haissinski
I	σ_s	σ_ϵ	σ_s	σ_ϵ	σ_s	σ_ϵ	σ_s
mA	cm	MeV	cm	MeV	cm	MeV	cm
0.09	0.56	3.47	0.56	3.46	0.56	3.45	0.56
0.18	0.64	3.49	0.64	3.46	0.64	3.46	0.64
0.27	0.72	3.66	0.70	3.50	0.70	3.46	0.70
0.36	0.80	4.14	0.78	3.91	0.75	3.47	0.75

Table 6: Inductive Wake for $\alpha = 5 \cdot 10^{-5}$, simulation results for QGF=1 mm, $N_{\text{par}} = 100\,000$, and bin width 0.15 mm compared with the result obtained by the Haissinski equation. The design current is 0.09 mA (see first row). The meaning of "smooth" is explained on page 6, m is 3.

The results for $\alpha = 7 \cdot 10^{-5}$ were analogous to the above. For the design current a rms bunch length of 0.62 cm was obtained. The momentum compaction factor $\alpha = 2.7 \cdot 10^{-4}$ lead to a bunch lengthening in the range of three percent.

5.2 Resistive Wall

An extensive study of the effect of the resistive wall wake fields has been done.
First of all the results of the Haissinski equation when using the wake of a 1 mm Gaussian bunch as a QGF for the three studied cases of the momentum compaction factor α are presented (Table 7).

α	I / mA	0.0	0.09	0.18	0.27	0.36	0.45	0.54	0.63	0.90	1.44
$5 \cdot 10^{-5}$	σ_s / cm	0.44	0.47	0.51	0.54	0.57	0.60	0.63	0.65	0.72	0.83
$7 \cdot 10^{-5}$		0.51	0.54	0.57	0.60	0.63	0.65	0.68	0.70	0.76	0.86
$27 \cdot 10^{-5}$		1.02	1.03	1.04	1.05	1.06	1.07	1.08	1.10	1.13	1.19

Table 7: Resistive Wall: Haissinski equation results, $\alpha = 5 \cdot 10^{-5}$, $\alpha = 7 \cdot 10^{-5}$, and $\alpha = 2.7 \cdot 10^{-4}$.

Figure 9 shows two results. The larger distortion of the bunch with the smaller compaction factor value at a comparatively lower beam intensity can easily be seen. A common feature is that the distributions "lean forward" so that the parasitic energy loss, a consequence of the real (resistive) part of the impedance, is compensated by the rf-voltage.

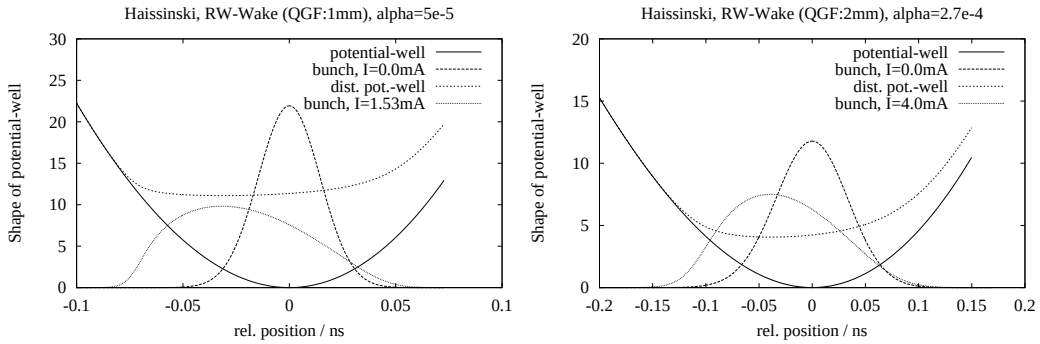

Figure 9: Resistive Wall Wake. Shape of the potential well and the bunch according to the solution of the Haissinski equation. On the left for $\alpha = 5 \cdot 10^{-5}$ and the for the zero current and $I = 1.53\,\mathrm{mA}$, on the right for $\alpha = 2.7 \cdot 10^{-4}$ and for the zero current and $I = 4.0\,\mathrm{mA}$.

The simulation results represented in Table 8, all for $\alpha = 7 \cdot 10^{-5}$, confer extremely well to those obtained by the Haissinski equation. It is interesting to note that although the number of particles varied to a great extent as well as the width of the bins and the usage of the QGF this had in the presented cases hardly any influence on the obtained bunch lengths (which were as mentioned previously calculated as the average value over the last 500 turns, the total time spent in the damping ring corresponding to 3000 turns).

QGF	N_{par}	bin	I								
mm	10^3	mm	mA	0.09	0.18	0.27	0.36	0.45	0.54	0.63	0.90	1.44
2	20	0.75		0.55	0.58	0.61	0.64	0.66	0.69	0.71	0.77	0.89
2	80	0.15		0.55	0.58	0.60	0.63	0.65	0.68	0.70	0.76	0.87
1	80	0.07	σ_s	0.55	0.58	0.61	0.63	0.66	0.68	0.71	0.77	0.88
1	200	0.06	cm	0.55	0.58	0.61	0.63	0.66	0.68	0.70	0.76	0.87
0.5	100	0.20		0.55	0.58	0.61	0.63	0.66	0.68	0.71	0.77	0.88
0.5	200	0.10		0.55	0.58	0.61	0.63	0.66	0.68	0.71	0.77	0.87

Table 8: Resistive Wall: Tracking results, $N_{\mathrm{sec}} = 1$, $\alpha = 7 \cdot 10^{-5}$, bunch length for 0.0 mA in all cases: 0.52 cm.

The range onwards from $I = 1.53\,\mathrm{mA}$ was characterized by a simulation dependent rms energy spread of the bunch as can be seen in Table 9. The first three results, (A) – (C), seem to stipulate that a QGF with a smaller rms bunch length leads to a smaller threshold where the energy begins to rise. For example in the first case (A) the rms energy spread began only to get noticeably larger from $I = 3.69\,\mathrm{mA}$ onwards.

	I / mA	1.53	1.71	1.89	2.07	2.25	2.43	2.61	2.79	2.97
	H σ_s / cm	0.87	0.90	0.93	0.96	0.98	1.00	1.02	1.04	1.06
A	S σ_s / cm	0.88	0.91	0.94	0.97	0.99	1.02	1.04	1.07	1.09
	S σ_ϵ / MeV	3.47	3.47	3.47	3.47	3.47	3.47	3.47	3.47	3.48
B	S σ_s / cm	0.89	0.92	0.95	0.98	1.01	1.04	1.06	1.09	1.12
	S σ_ϵ / MeV	3.48	3.49	3.49	3.51	3.54	3.59	3.65	3.75	3.88
C	S σ_s / cm	0.91	0.94	0.98	1.02	1.05	1.09	1.12	1.15	1.18
	S σ_ϵ / MeV	3.61	3.70	3.84	3.96	4.09	4.21	4.33	4.48	4.58
D	S σ_s / cm	0.90	0.93	0.97	1.00	1.04	1.07	1.10	1.13	1.16
	S σ_ϵ / MeV	3.60	3.70	3.79	3.94	4.04	4.18	4.33	4.42	4.57
E	S σ_s / cm	0.88	0.91	0.94	0.97	0.99	1.02	1.05	1.07	1.10
	S σ_ϵ / MeV	3.51	3.52	3.53	3.55	3.56	3.59	3.62	3.64	3.68
A: QGF=2.0 mm, $N_{\mathrm{par}} = 200\,000$, $N_{\mathrm{sec}} = 1$, bins: 0.1 mm										
B: QGF=1.0 mm, $N_{\mathrm{par}} = 200\,000$, $N_{\mathrm{sec}} = 1$, bins: 0.075 mm										
C: QGF=0.5 mm, $N_{\mathrm{par}} = 200\,000$, $N_{\mathrm{sec}} = 1$, bins: 0.075 mm										
D: QGF=0.5 mm, $N_{\mathrm{par}} = 100\,000$, $N_{\mathrm{sec}} = 1$, bins: 0.2 mm										
E: QGF=0.5 mm, $N_{\mathrm{par}} = 100\,000$, $N_{\mathrm{sec}} = 2$, bins: 0.2 mm, smooth:5										

Table 9: Resistive Wall: Haissinski (H) & Simulation (S) results for $\alpha = 7 \cdot 10^{-5}$.

The differences that occur in respect to the rms bunch lengths are small by comparison. The result obtained by an intermediate calculation step per turn

(using two sections, $N_{\text{sec}} = 2$, but where the rf-power was only submitted in the first section and meaning that the resistive wall wake is split up over the two sections) showed no rise in the rms energy spread. The discrepancy in the energy spread could therefore be caused by numerical calculation instabilities. The simulation results for $\alpha = 5 \cdot 10^{-5}$ are similar to those for $\alpha = 7 \cdot 10^{-5}$. The design bunch current resulted in a bunch lengthening of approx. 3 to 4 mm, i.e. 10 % (see Table 10).
Again at higher current values there was a noticeable difference when using one section ($N_{\text{sec}} = 1$) and different QGFs, ie. 0.5 mm, 1 mm or 2 mm. In the second case the rms energy spread begins to grow at ca. 1.71 mA and for the third at 2.61 mA.
At the design current and when $\alpha = 2.7 \cdot 10^{-4}$ the resistive wall wake is next to negligible. The results in respect to the various QGFs and higher currents were analogous.

I / mA	0.0	0.09	0.18	0.27
σ_s / cm	0.44	0.48	0.51	0.55

Table 10: Resistive Wall: $\alpha = 5 \cdot 10^{-5}$ average simulation results.

5.3 Cavities

The wake due to the cavities is the smallest for all studied cases (see for example Figure 12).
The solutions of the Haissinski equation are shown in Table 11; a bunch shortening is evident.

I / mA	0.0	0.09	0.27	0.45	0.63	0.81	0.99	1.53
σ_s / cm	0.44	0.43	0.42	0.40	0.39	0.38	0.37	0.34
σ_s / cm	0.52	0.51	0.50	0.49	0.47	0.46	0.45	0.42
σ_s / cm	1.01	1.01	1.00	0.99	0.98	0.97	0.96	0.94

Table 11: Cavities: Haissinski results, $\alpha = 5 \cdot 10^{-5}$, $\alpha = 7 \cdot 10^{-5}$, and $\alpha = 2.7 \cdot 10^{-4}$ using 2 mm QGF.

5.4 Fast Kicker

The effect of the fast kicker wake is such that it leads at lower currents to a a bunch shortening as would be expected of a capacitive wake. A minimum bunch length is obtained in all three cases at a current of approximately

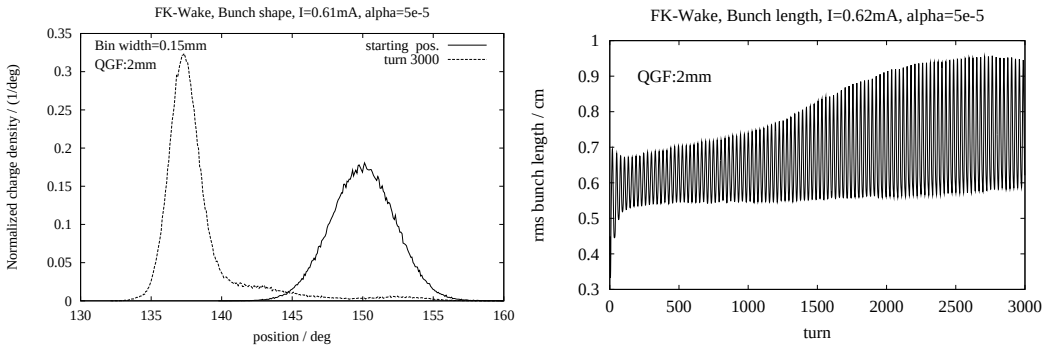

Figure 10: Results using the wake of the fast kickers. On the left the bunch shape ($I = 0.61\,\mathrm{mA}$) and on the right the development of the rms bunch length ($I = 0.62\,\mathrm{mA}$) over 3 000 turns starting with zero current distribution. In both cases: $\alpha = 5 \cdot 10^{-5}$; 200 000 macroparticles were used.

0.40 mA (solution of the Haissinski equation as well as for the simulation). An extreme rise in bunch length can be seen at ca. 0.60 mA. These results confer to the predicted solutions of the Haissinski equation (compare Table 12). The bunch lengthening can be explained by the appearance of a second potential-well minimum.

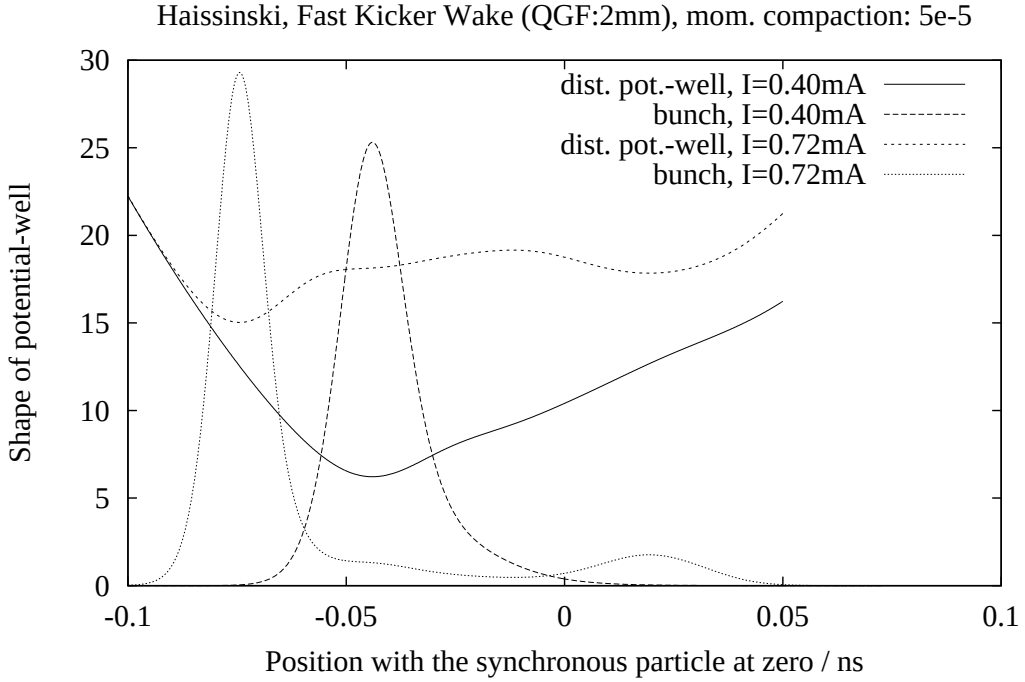

Figure 11: Two solutions of the Haissinski equation for the wake of the fast kicker and $\alpha = 5 \cdot 10^{-5}$.

For $\alpha = 5 \cdot 10^{-5}$: At $I = 0.54\,\mathrm{mA}$ the bunch has a length of ca. $\sigma_s = 0.40\,\mathrm{cm}$, the energy spread begins to rise and at $I = 0.58\,\mathrm{mA}$ ($\sigma_s = 0.50\,\mathrm{cm}$) the average position of the bunch is unstable. At $I = 0.63\,\mathrm{mA}$ the bunch is "lost".
For $\alpha = 2.7 \cdot 10^{-4}$, $I = 0.72\,\mathrm{mA}$ one obtains: $\sigma_s = 1.14\,\mathrm{cm}$ and $\sigma_\epsilon = 3.73\,\mathrm{MeV}$. Further the rms value of the average bunch position was 7.62 deg ($I = 0.63\,\mathrm{mA}$: 0.34 deg and at $I = 0.27\,\mathrm{mA}$: $2.6 \cdot 10^{-2}$ deg) therefore indicating that the bunch was undergoing a larger fluctuation in respect to its position.

α	I / mA	0.0	0.09	0.18	0.27	0.36	0.45	0.54	0.63	0.72
$5 \cdot 10^{-5}$		0.44	0.40	0.37	0.35	0.33	0.32	0.37	0.57	0.84
$7 \cdot 10^{-5}$	σ_s / cm	0.51	0.49	0.46	0.44	0.42	0.42	0.44	0.53	0.71
$27 \cdot 10^{-5}$		1.01	1.01	1.00	1.00	1.00	1.00	1.01	1.02	1.04

Table 12: Fast kickers: results of the Haissinski equation, $\alpha = 5 \cdot 10^{-5}$, $\alpha = 7 \cdot 10^{-5}$, and $\alpha = 2.7 \cdot 10^{-4}$ using 2 mm QGF.

α	I / mA	0.0	0.09	0.18	0.27	0.36	0.45	0.54	0.63	0.72
$5 \cdot 10^{-5}$		0.44	0.41	0.38	0.36	0.34	0.35	0.41	inst	inst
$7 \cdot 10^{-5}$	σ_s / cm	0.52	0.49	0.47	0.45	0.44	0.44	0.47	0.57	inst
$27 \cdot 10^{-5}$		1.06	1.06	1.05	1.05	1.06	1.06	1.07	1.08	1.14

Table 13: Fast kickers, simulation: average results using 2 mm/3 mm QGF, $N_{\mathrm{sec}} = 1$ (instability is abbreviated by "inst").

I / mA	0.45	0.495	0.54	0.585	0.60	0.61	0.62
σ_s / cm	0.35	0.36	0.41	0.50	0.54	0.59	0.74
σ_ϵ / MeV	3.52	3.53	3.54	3.55	3.59	3.71	4.80

Table 14: Fast kickers, simulation: result for $\alpha = 5 \cdot 10^{-5}$ using 2 mm QGF, $N_{\mathrm{sec}} = 1$, width of the bins: 0.02 cm, $N_{\mathrm{par}} = 200\,000$.

5.5 The total wake

The main component contributing to the total wake seen by the particles in the damping ring for the momentum compaction factors $\alpha = 5 \cdot 10^{-5}$ and $\alpha = 7 \cdot 10^{-5}$ is the one due to the inductive impedance followed by that of the fast kickers, whereas for a 1 cm Gaussian bunch ($\alpha = 27 \cdot 10^{-5}$) it is vice versa.

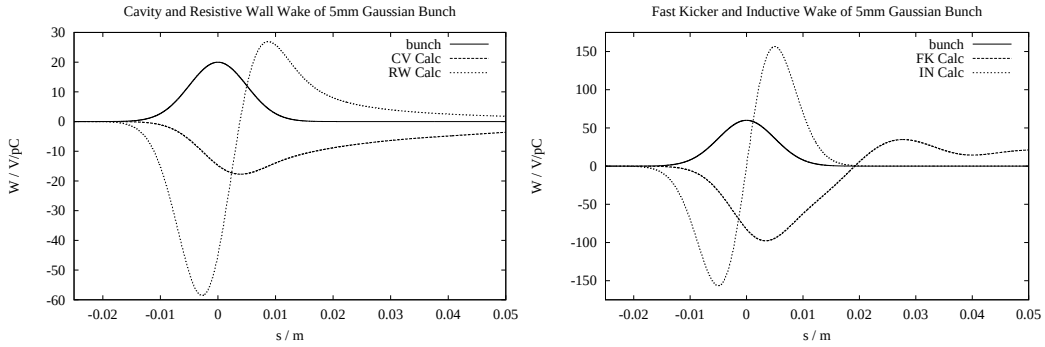

Figure 12: The wake components of a 5 mm (above) and a 1 cm (below) Gaussian bunch. On the left: the wake of the cavities and the resistive wall, on the right the fast kickers and the inductive wake.

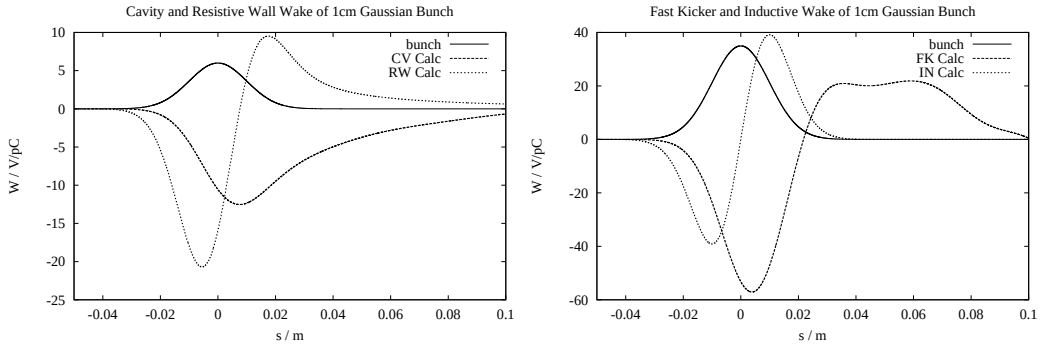

Figure 13: The wake field (all components) of a 5 mm and a 1 cm Gaussian bunch.

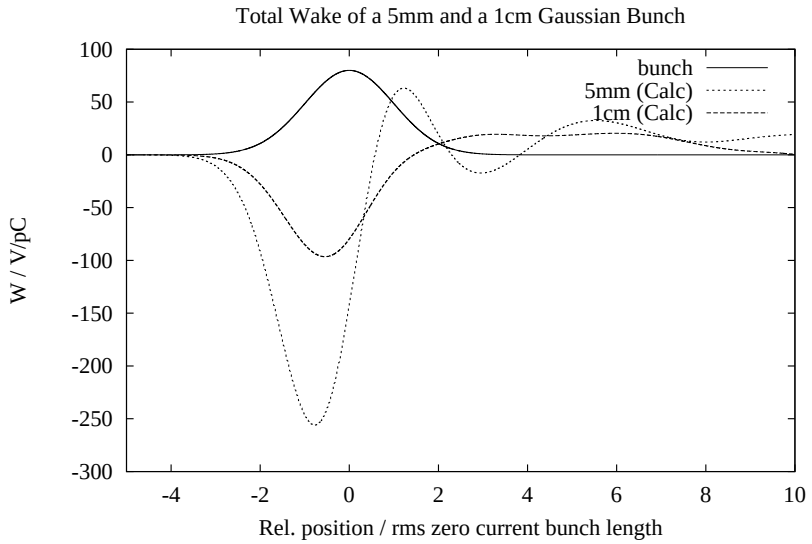

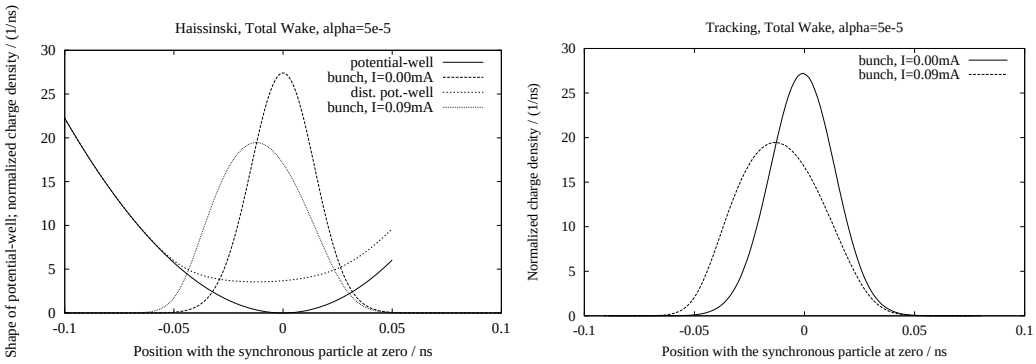

Figure 14: Total wake for $\alpha = 5 \cdot 10^{-5}$, design current. (a) Shape of the potential-well and the normalized charge density according to the Haissinski equation. (b) The average normalized charge density over the last 500 turns as seen by a tracking run. 100 000 macroparticles were used.

The results for the total wake are to be found in Tables 15, 16, and 17.
Analogous to the inductive wake, using an intermediate step per turn in the calculations ($N_{\mathrm{sec}} = 2$, with only the resistive wall and inductive wake split over the two sections) did not lead in the studied cases to an energy rise. This was not the case for currents of and above $I = 0.27\,\mathrm{mA}$ when using only one section ($N_{\mathrm{sec}} = 1$). Note that the same applies when using two sections and where none of the wakes are split up, i.e. the macroparticles see all of the wake and the rf in the first section, so that only the damping and quantum excitation terms play a role in the second part.
The results for two sections which are shown are those where the smoothing technique (see page 6) was applied. Using the usual (basic) method lead to no noteworthy differences.

	$N_{\mathrm{sec}} = 1$		$N_{\mathrm{sec}} = 1$ smooth: 5		$N_{\mathrm{sec}} = 2$ smooth: 5		Haissinski
I	σ_s	σ_ϵ	σ_s	σ_ϵ	σ_s	σ_ϵ	σ_s
mA	cm	MeV	cm	MeV	cm	MeV	cm
0.09	0.56	3.47	0.56	3.47	0.56	3.46	0.56
0.18	0.64	3.48	0.64	3.47	0.64	3.47	0.64
0.27	0.74	3.83	0.73	3.72	0.71	3.47	0.71
0.36	0.85	4.54	0.84	4.33	0.78	3.48	0.77

Table 15: The total wake, $\alpha = 5 \cdot 10^{-5}$. Average simulation results using an 1 mm inductive QGF, a 0.5 mm resistive wall QGF, a 2 mm fast kicker QGF, 0.5/1.0 mm cavity QGFs, and $N_{\mathrm{par}} = 100\,000/200\,000$ (width of the bins: 0.20 mm) compared with the result obtained by the Haissinski equation. The design current is 0.09 mA.

The bunch lengthening factors for the design current were equivalent to those for the purely inductive wake. This was also the case for $I = 0.18\,\mathrm{mA}$.
For $\alpha = 5 \cdot 10^{-5}$ the simulation bunch centre at the design current differed by ca. one and a half degrees from the synchronous phase (150.0 deg). The result depended slightly on the number of sections used, being ca. 148.3 deg. ($N_{\mathrm{sec}} = 1$) and 148.6 deg for two sections.

	$N_{\mathrm{sec}} = 1$		$N_{\mathrm{sec}} = 1$ smooth: 5		$N_{\mathrm{sec}} = 2$ smooth: 5		Haissinski
I	σ_s	σ_ϵ	σ_s	σ_ϵ	σ_s	σ_ϵ	σ_s
mA	cm	MeV	cm	MeV	cm	MeV	cm
0.09	0.62	3.48	0.62	3.48	0.61	3.47	0.62
0.18	0.69	3.49	0.70	3.49	0.68	3.47	0.69
0.27	0.80	3.93	0.79	3.76	0.75	3.48	0.75
0.36	0.94	4.68	0.94	4.56	0.81	3.48	0.82

Table 16: The total wake, $\alpha = 7 \cdot 10^{-5}$. Average simulation results for using an 1 mm inductive QGF, a 0.5 mm resistive wall and cavity QGF, a 2 mm fast kicker QGF, and $N_{\mathrm{par}} = 100\,000/200\,000$ (width of the bins: 0.20 mm) compared with the result obtained by the Haissinski equation. The design current is 0.09 mA (see first row).

	$N_{\mathrm{sec}} = 1$		$N_{\mathrm{sec}} = 1$ smooth: 5		$N_{\mathrm{sec}} = 2$ smooth: 5		Haissinski
I	σ_s	σ_ϵ	σ_s	σ_ϵ	σ_s	σ_ϵ	σ_s
mA	cm	MeV	cm	MeV	cm	MeV	cm
0.00	1.06	3.59	1.06	3.59	1.00	3.51	1.02
0.09	1.09	3.59	1.09	3.59	1.03	3.52	1.05
0.18	1.13	3.59	1.13	3.58	1.07	3.52	1.09
0.27	1.24	3.87	1.23	3.85	1.10	3.53	1.13
0.36	1.42	4.44	1.42	4.42	1.14	3.54	1.17

Table 17: The total wake, $\alpha = 2.7 \cdot 10^{-4}$. Average simulation results using an 1 mm inductive, resistive wall, and cavity QGF, a 3 mm fast kicker QGF, and $N_{\mathrm{par}} = 100\,000/200\,000$ (width of the bins: 0.40 mm) compared with the result obtained by the Haissinski equation. The design current is 0.09 mA.

6 Comparison and Conclusion

6.1 SLC Damping Ring

Tracking simulations have been applied to the SLC damping rings (the old chamber but with bellow sleeves) and compared to the results in [19]. Beyond a threshold current of $3.0 \cdot 10^{10}$ the energy spread of the beam in the old SLC damping ring increased and a "saw-tooth instability" appeared. The possibility of such an instability occurring was shown by T. Weiland in his tracking studies in 1981 (see [4]).

$N/10^{10}$	σ_s/σ_{s0}	$\sigma_\epsilon/\sigma_{\epsilon 0}$	$-<s>/\sigma_{s0}$
1	1.27	1.00	0.41
2	1.47	1.01	0.61
3	1.62	1.04	0.76
4	1.77	1.11	0.86
5	1.97	1.30	0.92
6	2.14	1.46	0.97

Table 18: SLC Damping Ring. Average bunch properties vs N.

In the simulations the real damping time was used, there therefore being 15 142 turns per damping time. The program was started with the zero current distribution for $N = 1$, 2, and $3{\cdot}10^{10}$ and ran for 45 000 turns (ca. three damping times). The higher currents used the last position on the previous run with the next smaller current as the starting position. In all cases the number of macroparticles N_{par} used was 100 000.

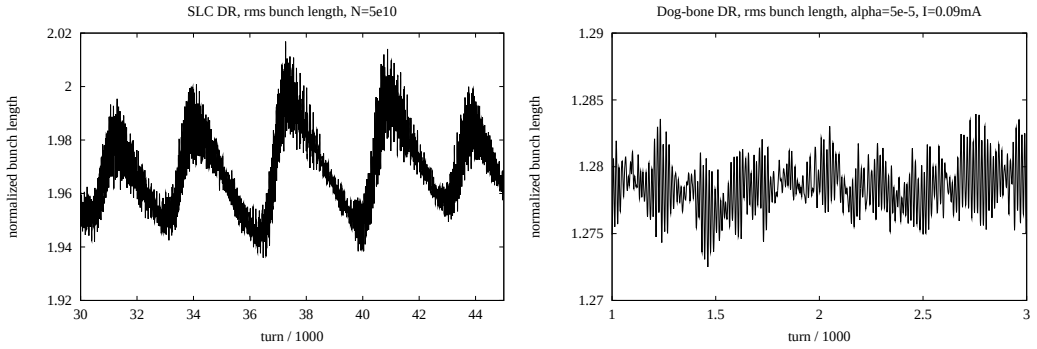

Figure 15: Turn-by-turn normalized rms bunch length σ_s/σ_{s0}. On the left for the SLC DR, $N = 5 \cdot 10^{10}$, and on the right for the dog-bone DR, design current (using $N_{\mathrm{sec}} = 2$). In both cases 100 000 macroparticles were used. Note that the bunch length scaling for the SLC is a factor five larger.

The results for the rms bunch length and the shift of the bunch centre confer extremely well to those of Karl Bane ([19]). At the current, $5.0 \cdot 10^{10}$, a

reasonably regular overshoot pattern in the moments as function of time could be seen, too (see Figure 15). Here the bunch length varied about 4 % over a cycle. The lengthening time was about $11/\nu_{s0}$ and the shortening time was slightly more than twice as long.
Going on the above stated good correspondence between the results of the two tracking programs and with the measurements those of the presented tracking studies for the dog-bone damping ring seem to be trustworthy.

6.2 Dog-bone Damping Ring

One must not forget that the results for the dog-bone DR are based on an impedance model which was originally assumed for a 1 cm bunch. The effects of the components such as the bellows and BPMs which contributed here only to inductive impedance may be different and thereby bring about different results. Naturally in future further studies will be needed based upon an improved impedance model.
Returning to the used impedance model one can however state that in all cases the tracking studies for the total wake give cause to assume that the bunches would be stable under such conditions. Whereas the bunch shape was only slightly changed for $\alpha = 2.7 \cdot 10^{-4}$, the bunches corresponding to the two smaller momentum compaction factors studied undergo a large bunch lengthening effect at the design current of 0.09 mA (20 % to 30 %) due to the inductive impedance. The turn-by-turn rms bunch length values are quite stable as can be seen by the example ($\alpha = 5 \cdot 10^{-5}$) shown in Figure 15 and is quite typical. At the design current but also for the fourfold current, $I = 0.36$ mA, the turn-by-turn the bunch length varied by ca. 0.02 %.
Studies applied to the dog-bone DR parameters as in the CDR-report (circumference 17 km) where the total wake was modified accordingly show similar results, the bunch lengthening being somewhat smaller.

Acknowledgements

The author is most grateful to K. Bane for being so kind as to supply the quasi-Green's function wake so that a comparison to his results for the SLC damping ring was possible.
He would further like to thank Reinhard Brinkmann, Rainer Wanzenberg and Thomas Weiland for the fruitful discussions and their suggestions.

References

[1] V. D. Shiltsev, *TESLA Damping Ring Impedances: Preliminary Design Consideration*, DESY–TESLA 96-02 (1996)

[2] *Conceptual Design of a 500 GeV* e^+e^- *Linear Collider with Integrated X-ray Laser Facility*, DESY 1997-048

[3] M. Sands, *The Physics of Electron Storage Rings. An Introduction*, SLAC-0121 (1970)

[4] T. Weiland, *On the quantitative prediction of bunch lengthening in high energy electron storage rings*, DESY 81-088 (1981)

[5] J. Haissinski, Nuovo Cimento 18 B (1973) 72

[6] T. Okugi, et. al, *Impedance Measurement Utilizing Bunch Lengthening Effect in ATF Damping Ring*, ATF 97-23

[7] R. L. Holtzapple, *Longitudinal Dynamics at the Stanford Linear Collider*, SLAC-Report-487 (1996)

[8] S. Heifets, et. al, SLAC/AP-99 (1995)

[9] B. Zotter, *A review of Self-consistent Integral Equations for the Stationary Distribution in Electron Bunches*, KEK-Report 90-21 (1991)

[10] A. Chao, *Physics of Collective Beam Instabilities in High Energy Accelerators*, John Wiley & Sons, Inc. (1993)

[11] D. Boussard, CERN Lab II/RF/Int 75-2 (1975)

[12] H. Wiedemann, *Particle Accelerator Physics: 2: Nonlinear and Higher Order Beam Dynamics*, Springer (1995)

[13] KEK *B-Factory Design Report*, KEK-Report 95-7 (1995)

[14] K. Bane, *The calculated longitudinal impedance of the SLC Damping Rings*, EPAC 1988

[15] H. Schlarb, *Resistive Wall Wake Fields*, DESY–TESLA, 97-22 (1997)

[16] *JLC Design Study*, KEK-Report 97-1 (1997)

[17] B. Grishanov, et. al, *Very Fast Kicker for Accelerator Applications*, DESY–TESLA 96-11 (1996)

[18] Michaela Marx, private communication

[19] K. Bane and K. Oide, *Simulations of the longitudinal instability in the SLC damping rings*, SLAC-PUB-6216